7A.1 SPECTRAL PROCESSING TECHNIQUES FOR MEASURING DOPPLER VELOCITY OF RAINFALL FROM A LOW EARTH ORBITING SATELLITE

Simone Tanelli[1*], Eastwood Im [1], Stephen L. Durden [1], and Luca Facheris [2]
[1] Jet Propulsion Laboratory, California Institute of Technology, Pasadena CA, USA
[2] Dipartimento di Ingegneria Elettronica - Università di Firenze - Firenze - Italy

1. INTRODUCTION

The importance of the motion of air masses at all scales of atmospheric circulation has brought substantial development of the Doppler radar technology in the field of precipitation monitoring. Although techniques have been developed in the last two decades for ground-based and airborne Doppler weather radars they do not fully address the issues pertained to spaceborne radars. These unique issues arise from the downward viewing geometry with a fast moving (*i.e.,* $v_S \cong 7$ km/s for Low Earth Orbiting (LEO) satellites) orbiting platform and a relatively large volume of resolution (*e.g.*, 2km footprint radius and 250m range resolution).

The spaceborne precipitation radar studied in this paper (referred to as Nadir-looking Doppler Precipitation Radar - NDPR) is cross-track scanning with a small scan angle β (*e.g.*, $\beta < 5$ deg.). This viewing geometry allows to measure the average vertical motion v_R of the hydrometeors by calculating the first moment of the measured Doppler velocity spectrum. Measurements of v_R are affected by several errors such as:

Errors of the spectral moment estimator (SME): The estimate of the first spectral moment calculated from the returns of *M* radar pulses is a random variable typically described through its expected value $< v >$ and standard deviation $\sigma(v)$. When the Doppler spectrum is Gaussian, the statistics of *x* can be calculated from the following parameters: a) the Signal to Noise Ratio (*SNR*), b) the normalized mean Doppler velocity $v_N = v\ 2\ /\ (\lambda\ PRF)$ where *PRF* is the radar Pulse Repetition Frequency and λ is the radar operating wavelength, c) the number of samples *M*. and d) the normalized width $w_N = w\ 2\ /\ (\lambda\ PRF)$ where *w* is the Doppler velocity spectral width of the signal. The last is probably the most critical parameter in a LEO Doppler radar design. In fact, $w^2 = w_S^2 + w_R^2$ where w_R is the spread due to turbulence, wind shear and different terminal velocities (typically less than 5 m/s) and $w_S = 0.3\ v_S\ \theta_3$ (where θ_3 is the antenna beamwidth) is the spread due to the spacecraft motion (Amayenc et al. 1993). By approximating $\theta_3 \cong \gamma\ \lambda/D$, where *D* is the antenna diameter and $\gamma \sim 1.25$, it follows that, given a choice of D, w_N does not depend significantly on λ as long as $w_S >> w_R$. When w_S is comparable to w_R, instead, smaller λ lead to larger w_N because w_R does not depend on λ.

* *Corresponding author address:* Simone Tanelli, Jet Propulsion Laboratory, 4800 Oak Grove Dr. MS 300-243, Pasadena CA 91109; e-mail: simone.tanelli@jpl.nasa.gov

Table 1 shows the w_N corresponding to some feasible radar configurations assuming $w_R = 0$.

- *NUBF-induced bias:* when the radar is observing a non-homogeneous rainfall field, the contributions to the Doppler spectrum from different portions of the resolution volume are unevenly weighted. Since each rain target is subject to a Doppler shift proportional to its along-track displacement with respect to the cross-track plane, the inhomogeneous weighting modifies the shape of the Doppler spectrum and induces a bias in the estimates of vertical velocity.
- *Pointing-induced bias:* The pointing-induced offset in Doppler velocity is $v_P = \boldsymbol{i_V} \bullet \boldsymbol{i_X} v_S$ where $\boldsymbol{i_x}$ is the along-track direction and $\boldsymbol{i_v}$ is the radar pointing direction. For $v_s = 7$ km/s , the rms in the knowledge of the pointing direction should be of 4 arcsecs or less in order to guarantee $|v_P| < 1$ m/s. Such requirement for a LEO satellite poses a technological challenge.

2. PERFORMANCES OF STANDARD SPECTRAL MOMENTS ESTIMATORS

The two most widely used categories of Spectral Moments Estimators (SME) of weather radar signals are the Pulse Pair (PP) processing and the spectral analysis through Discrete Fourier Transform (DFT). Their performances have been analyzed focusing on their application to spectra measured by NDPR (Tanelli et al. 2002). The results of these studies are summarized here for four DFT-based SME and for the Pulse Pair (PP) algorithm. The four DFT-SME differ in their ways of handling of noise and defining the initial guess, in general the mean velocity estimate is:

$$\hat{v} = -\frac{\lambda PRF}{2M} m_0$$

$$m_0 = \left\{ \begin{array}{l} m_0' + \dfrac{\sum_{m=m_0'-M/2}^{m_0'+M/2} (m - m_0') \cdot \left[\tilde{P}_{\mathrm{mod}_M(m)} - \hat{N}_{\mathrm{mod}_M(m)} \right]}{(S_S + S_N) - \hat{S}_N} \cdot \\ . \end{array} \right\} \quad (1)$$

***D* [m]**	***2***	***3***	***4***	***5***	***6***	***10***
PRF						
5000	0.50	0.34	0.25	0.20	0.17	0.10
6000	0.42	0.28	0.21	0.17	0.14	0.09
7000	0.36	0.24	0.18	0.14	0.12	0.07
8000	0.32	0.21	0.16	0.13	0.11	0.06

Table (1): Normalized spectral widths w_N as function of (*PRF* and antenna diameter D) for $v_s = 7000$ m s^{-1} and $w_R = 0$.

where S_S and S_N are the signal and noise power, respectively, $\hat{S}_N$ is the estimated mean noise power, P_m is m-th line of the power spectrum as calculated through DFT of M complex voltage samples (*periodogram*), $\hat{N}_m = \hat{S}_N / M$ is the estimated noise spectral density, and m_0' is the number of a specific frequency bin in which the initial estimate α of the mean spectral frequency is made (i.e., $m_0' = \alpha M / PRF$).

The first algorithm (DFT-Z) assumes $m_0' = 0$. It does not remove any white noise contribution (*i.e.*, $\hat{S}_N = 0$ in (1)), which makes it a biased estimator at low SNR's. The second algorithm (DFT-ZN) also assumes $m_0' = 0$ but it removes the nominal power (*i.e.*, $\hat{S}_N = S_N$) in order to eliminate the bias due to white noise. As shown by Sirmans and Bumgarner (1975), at low SNR's the standard deviation of (1) for DFT-ZN is significantly higher than that for DFT-Z.

The third algorithm (DFT-M) was suggested by Zrnic (1979). Here m_0' is the number of the frequency bin which has the largest power (*i.e.*, $m_0' : P_{m_0} = \max\{P_k\}$), and it does not remove any white noise contribution. For narrow spectra (*e.g.*, $w_N < 0.1$) and large M (e.g., M>1000), this algorithm provides unbiased estimates of the first spectral moment with the corresponding

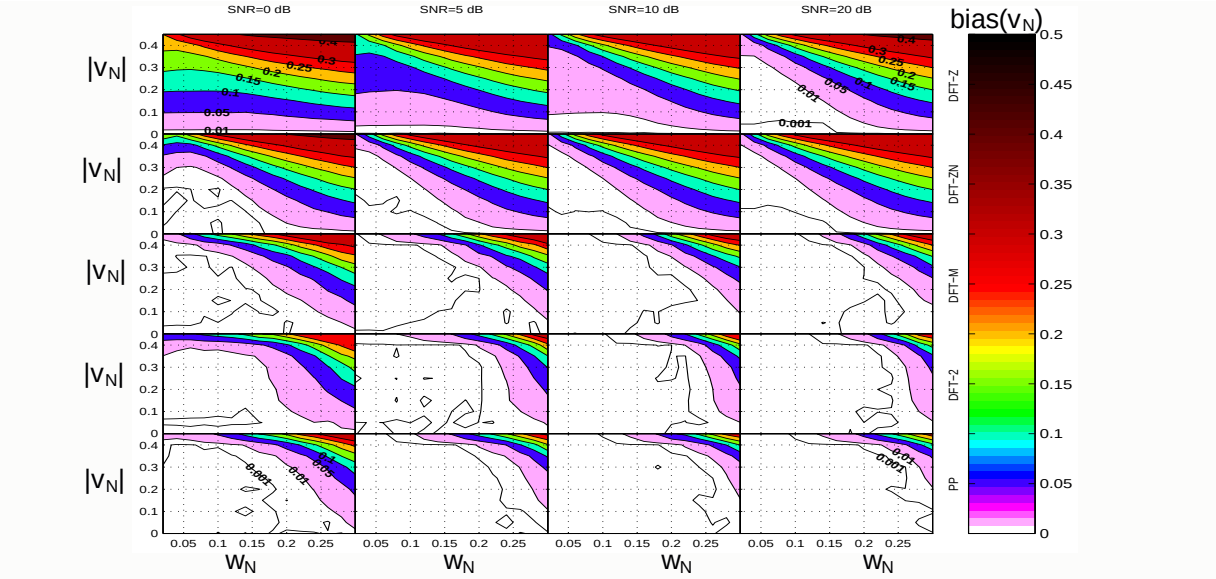

Figure 1: Bias on normalized mean velocity estimates for 5 SME algorithms. In the simulations M=64.

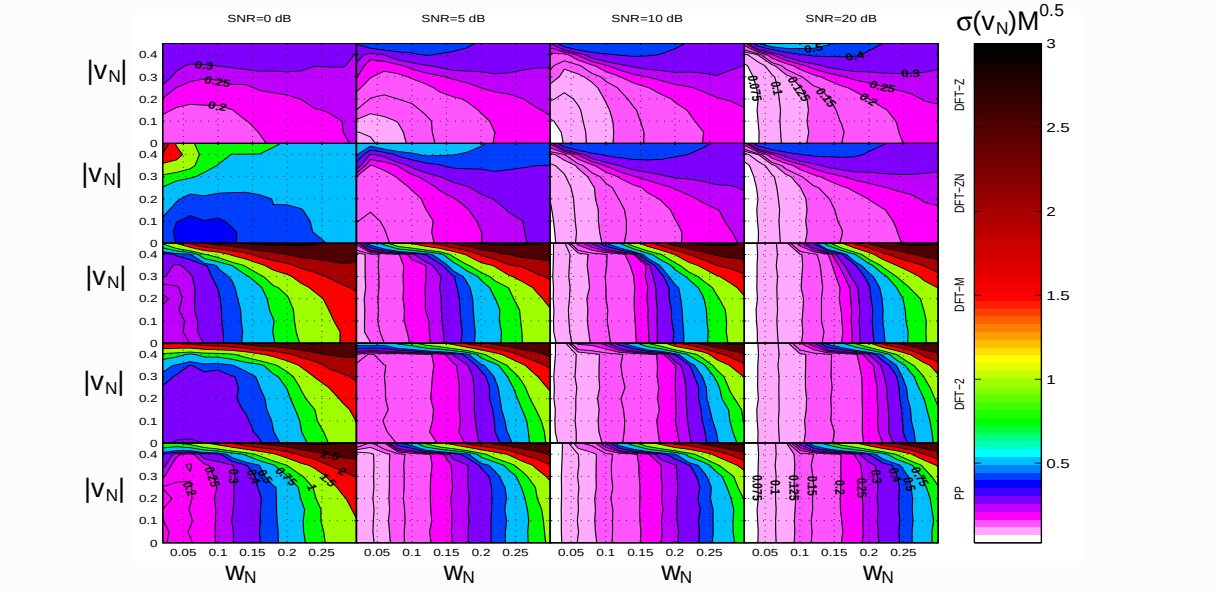

Figure 2: Normalized standard deviation of normalized mean velocity estimates for 5 SME algorithms. The standard deviation is scaled by $M^{0.5}$: such quantity is invariant on M for DFT-Z, DFT-ZN and PP.

standard deviations comparable to those obtained by DFT-Z. However, this algorithm is more sensitive to w_N than DFT-Z and DFT-ZN (Tanelli et al. 2002b).

The fourth algorithm, referred to as 'two-step' DFT algorithm (DFT-2), was recently introduced by Tanelli et al. (2002) to provide better performances for spaceborne applications where w_N larger than 0.1 may occur. In the first step of this algorithm, (1) is applied with $m_0' = 0$ and $\hat{S}_N = S_N$ to obtain a first velocity estimate $\hat{v}^{(1)}$. $\hat{S}_N$ is then updated by setting it equal to the minimum of the smoothed periodogram. In the second step, a refined velocity estimate $\hat{v}^{(2)}$ is obtained through (1) with $m_0' = \hat{v}^{(1)}/(-\lambda PRF/2M)$ and with the updated $\hat{S}_N$. This second step can be repeated until $\left|\hat{v}^{(i)} - \hat{v}^{(i-1)}\right|$ falls below a specified threshold. In general, DFT-2 is capable of providing unbiased estimates with standard deviations comparable to DFT-Z.

Estimates of the mean velocity of Gaussian spectra simulated as in Tanelli et al. (2002b) were calculated through the four DFT-SME and through PP (contiguous pairs). The normalized bias and standard deviation of these estimates are shown in Figs. (1) and (2), respectively. While the estimates of DFT-Z and DFT-ZN are heavily biased by the aliased portions of the spectrum, those obtained through DFT-M, DFT-2 or PP are unbiased for a wide range of w_N and v_N. Among these, PP shows the smallest standard deviation for low SNR's and small w_N, DFT-2 shows the smallest standard deviation for high SNR's and $w_N \geq 0.1$, and DFT-M shows performances between those of PP and DFT-2.

All performances degrade rapidly when $|v_N|$ exceeds a threshold that depends on w_N and the specific SME algorithms used. It was found that such threshold can be approximated by $0.5 - A_R w_N$ where A_R is equal to 1 for DFT-2 and to 1.65 for DFT-M. One can consider as the 'nominal' performances of the algorithm those calculated for $|v_N|$ lower than this threshold.

3. COMBINED FREQUENCY TIME TECHNIQUE

As recently demonstrated by Tanelli et al. (2002), the bias in vertical velocity estimates induced by Nonuniform Beam Filling (NUBF) is proportional to the reflectivity gradient in the along-track direction and it can reach values of several m/s. Such bias affects equally all standard SME algorithms.

In order to remove such bias, the Combined Frequency Time (CFT) technique has been developed (Tanelli et al. 2003) and it is briefly recalled here. CFT aims at removing the NUBF-induced bias from the estimates of rainfall average vertical velocity by estimating the first moment of the tracks of rainfall distributed targets in the along-track satellite position / Doppler velocity *(x-v)* plane.

Figure 3 shows a sequence of periodograms measured for a fixed range cell. Each periodogram is calculated from the DFT of $M = 64$ complex voltage samples. Therefore one periodogram is obtained in the time T_I which corresponds to an along-track displacement of the satellite $\Delta_x = v_s M/PRF$. Provided that Δ_x is smaller than the antenna footprint, several consecutive periodograms include the spectral signature from the same target. Such signature shifts in Doppler along lines with slope v_s/h_s in the satellite along-track position vs. Doppler velocity (*x-v*) plane, leaving the 'target track'. The example in Fig. 3 is obtained from a typical NUBF situation where the power spectrum often deviates substantially from a Gaussian shape (see the example in panel c). On the other hand, it has been demonstrated that, for NDPR, the target tracks can be well approximated by a Gaussian (from the shape of the antenna pattern), regardless of NUBF. The first moment estimated through a DFT-SME of each target track provides accurate information on both the target position (when the target is in the antenna maximum gain direction) and its true vertical velocity. The last step of the CFT technique is a weighted moving average of the of the ensemble of target velocities to generate the final estimated velocity field.

Results of simulations confirmed that CFT is capable of removing the NUBF-induced bias and provide vertical velocity estimates with the accuracy predicted for DFT-2 with an equivalent number of samples, and independently of the presence of NUBF.

Furthermore, its application to surface Doppler spectra is useful to correct for the pointing-induced bias (Im et al 2002) which can be estimated through the apparent Doppler velocity of the sea surface. In general this could be achieved by means of any SME. However, spaceborne radars are typically operating at frequencies where signal attenuation induced by rain and other atmospheric constituents is not generally negligible. It follows that, under NUBF conditions, the non uniform path integrated attenuation can alter the shape of the Doppler spectrum and introduce a bias in the vertical velocity estimate as described in the previous section. In this situation, CFT can provide unbiased estimates of the apparent vertical velocity, and correct for the pointing induced bias.

Simulations were carried out using a 3D Doppler radar simulator (Tanelli et al., 2002) where several sequences of periodograms are simulated from high-resolution 3-D rainfall data sets acquired by the NASA/JPL Airborne Rain Mapping Radar (ARMAR). In this simulation model, each NDPR resolution volume (2.2-km horizontal and 240-m vertical resolution) is divided into several sub-volumes of sizes comparable to those of the ARMAR data (200-m horizontal and 80-m vertical resolution) to account for the presence of NUBF. The spacecraft attitude errors and antenna vibrations were assumed to have cutoff frequency at 0.25 Hz and an rms angle of 0.02°.

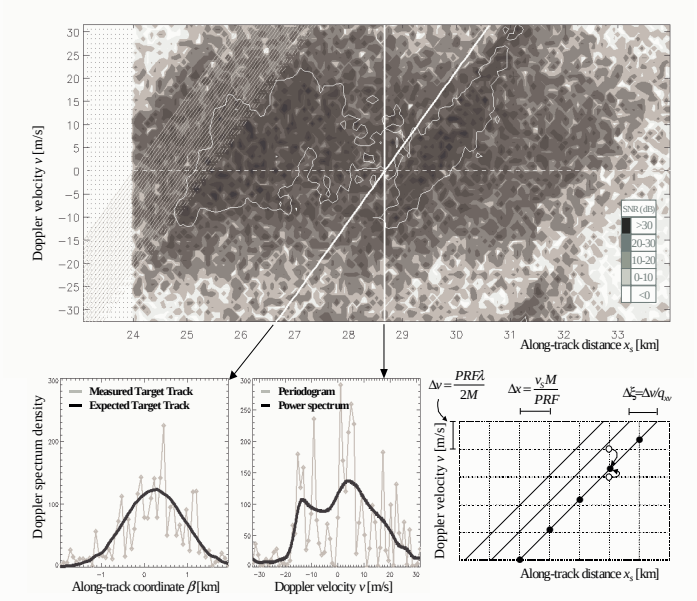

Fig. 3 Application of CFT to sequences of measured Doppler spectra: a) example of sequence of Doppler spectra for a fixed range bin, white diagonal lines indicate the target tracks, b) sample Gaussian target track, c) sample non-Gaussian periodogram, d) interpolation of power spectral samples to obtain measured target tracks.

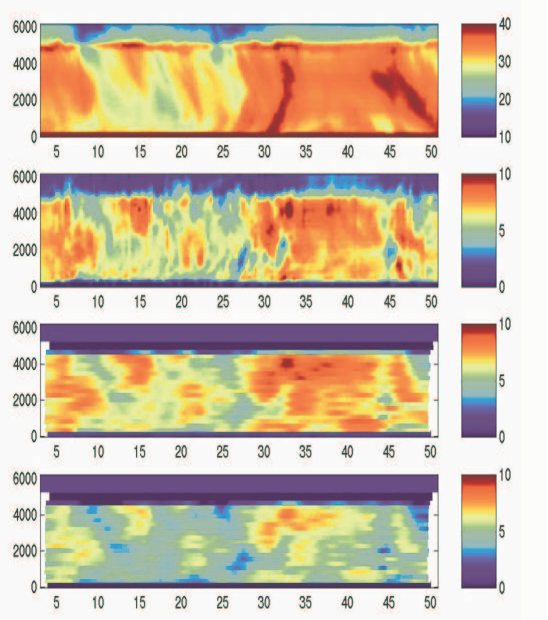

Fig 4 From top to bottom. ARMAR reflectivity field (dBZ), ARMAR vertical velocity (m s^{-1}), NDPR estimated vertical velocity through CFT with pointing-error correction, NDPR estimated vertical velocity through CFT without pointing-error correction. Vertical axis is altitude (m) and horizontal is along-track distance (km).

Figure 4 shows CFT results obtained from NDPR simulated signal from the ARMAR dataset of Hurricane Bonnie (true reflectivity and vertical velocity are shown in the first two panels). In this case study the performances of the standard SME were affected by the presence of NUBF-induced bias and their overall rms error was ~3.5 m s^{-1} even in absence of pointing errors. The vertical velocity field shown in the bottom panel was obtained by applying CFT directly to the Doppler spectra from the rain range gates without correcting first for the pointing-induced bias. In this case the pointing-induced bias is biasing the whole vertical velocity field by ~3 m/s. The vertical velocity field shown in the third panel was obtained by first correcting for the pointing-induced bias through CFT processing of the sea surface echo, and then applying CFT to the Doppler spectra from the rain range gates in order to correct for the NUBF-induced bias. The overall rms error in this case is of 0.92 m s^{-1} with no significant bias.

ACKNOWLEDGMENT

The research described in this paper was performed at the Jet Propulsion Laboratory, California Institute of Technology, under contract with the National Aeronautics and Space Administration, and by the University of Firenze.

REFERENCES

Amayenc P., J.Testud and M.Marzoug, 1993: Proposal for a spaceborne dual-beam rain Radar with Doppler capability, *J. Atm. Oce. Tech.*, **10**, pp.262-276.

Im E., S. Tanelli, R. Mascelloni and L. Facheris 2002: Spaceborne rainfall Doppler radar measurements: correction of errors induced by pointing uncertainties, Proc. of SPIE Vol **4894**-52, Hangzhou (RPC), Oct. 23-27 2002.

Sirmans D. and B. Bumgarner, 1975: Numerical comparison of five mean frequency estimators. *J. Appl. Meteor.*, **14**, 991-1003.

Tanelli S., E. Im, S. L. Durden, L. Facheris and D. Giuli, 2002: The effects of nonuniform beam filling on vertical rainfall velocity measurements with a spaceborne Doppler radar, *J. Atmos. Oceanic Technol.,* **19**, 1019-1034.

--, --, Luca Facheris and Eric A. Smith, 2002 DFT-based spectral moment estimators for spaceborne Doppler precipitation radar, Proc. of SPIE Vol. **4894**-50, Hangzhou (RPC), Oct. 23-27 2002.

--, --, --, -- D. Giuli and S.L.Durden, 2003: Rainfall Doppler velocity measurements from spaceborne radar: overcoming NUBF effects, *Accepted on Journal of Atmos and Oce. Tech.*

Zrnic D.S., 1979: Estimation of spectral moments for weather echoes. *IEEE Trans. On Geosc. Electr.*, **4**, 113-128.